Available online at www.sciencedirect.com
SCIENCE DIRECT®
Journal of Magnetic Resonance 164 (2003) 154–159
JMR Journal of Magnetic Resonance
www.elsevier.com/locate/jmr

Communication

Correlation functions for inhomogeneous magnetic field in random media with application to a dense random pack of spheres

B. Audoly,[a,b] P.N. Sen,[a] S. Ryu,[a] and Y.-Q. Song[a,*]

[a] *Schlumberger-Doll Research, Old Quarry Road, Ridgefield, CT 06877-4108, USA*
[b] *Laboratoire de modélisation en mécanique, Université Pierre et Marie Curie, 75231 Paris Cedex 05, France*

Received 5 March 2003; revised 6 May 2003

Abstract

In porous media subject to applied magnetic field, the internal field arises out of susceptibility contrast of the constituents. We have examined the spatial inhomogeneity of the internal fields in a random pack of spheres using numerical computation. We find that the pair-correlation function of the internal field (K_2) is a close approximation to the structure factor of the material, thus K_2 can be used to characterize pore geometry. The magnetic length scale Λ_M exhibited in K_2 is shown to be related to the fluid transport in the medium.

Keywords: NMR; Internal magnetic field; Correlation function; Structure factor

1. Introduction

The internal structures of many complex materials are vital for their properties. For instance, the amount of the solid bone tissue and its spatial structure are critical for the bone strength. Inorganic porous media such as rocks, concretes, and soils may allow transport of fluids depending on their porosity and pore sizes. We take the approach that the internal field due to the susceptibility contrast of the constituent materials carries a fingerprint of the internal structure of the materials [1]. Therefore, various magnetic relaxation phenomena which probe this internal field are potentially useful to unfold the pore geometry. Such internal field inhomogeneity was first recognized by Brown [2]. He computed the magnetic field distributions from a single magnetized grain and a random packing of grains, and also observed the effects of such distributions on the decay of NMR signals. Drain [3] studied the NMR line broadening due to field inhomogeneities in a powdered sample. He computed the field distribution arising from nearest neighbor spheres (and other shapes) in a cubic close packing. Sen and Axelrod [4] recently reviewed the literature on internal fields while computing it for a pack of cylinders. The effects of the internal field have since been observed [5–8] mostly by its contribution to transverse spin–spin relaxation and characterized by a very wide distribution of gradients.

The purpose of this paper is to study statistical features of the local magnetic field and show that they are closely related to the corresponding attributes of the geometry. In particular, we show a close correspondence of the two-point correlation function of the internal field and that of the pore space. Two-point correlation function is a fundamental attribute [9] of the structure and determines static scattering of light, X-ray, and neutrons by the object.

2. Structure factor and correlation functions

The structure factor or the pair-correlation function $S_2(\mathbf{r})$ of a porous material is defined as a macroscopically averaged quantity [10]:

$$S_2(\mathbf{r}) \equiv \frac{1}{V_p} \int d\mathbf{r}_1 X(\mathbf{r}_1 + \mathbf{r}) X(\mathbf{r}_1). \quad (1)$$

* Corresponding author. Fax: 1-203-438-3819.
E-mail address: ysong@slb.com (Y.-Q. Song).

1090-7807/$ - see front matter © 2003 Elsevier Science (USA). All rights reserved.
doi:10.1016/S1090-7807(03)00179-4

Here V_p is the the pore volume and the function $X(\mathbf{r})$ is defined to be unity in the pore space and zero otherwise. Thus, $\int d\mathbf{r}X(\mathbf{r})/V_p = 1$. We will assume that the sample is homogeneous and isotropic, so $S_2(\mathbf{r})$ is only a function of $|\mathbf{r}|$. Note that the definition implies that $S_2(\mathbf{r}) \geqslant 0$ and also its Fourier transform is positive definite.

First consider the limiting behavior of $S_2(\mathbf{r})$:

$$\frac{1}{V_p}\int d\mathbf{r}S_2(\mathbf{r}) = 1, \tag{2}$$

$$S_2(0) = 1, \tag{3}$$

$$S_2(\infty) = \phi, \tag{4}$$

$$\left.\frac{dS_2(\mathbf{r})}{dr}\right|_{r=0} = -\frac{S}{4V_p}. \tag{5}$$

Here, S is the total surface area of the sample and ϕ is the porosity. The proof of the last identity can be found in [10,11]. There is an implicit angular average and the sample is assumed to be isotropic. To incorporate the limiting behavior of S_2, we define the normalized pair-correlation function f as

$$S_2(\mathbf{r}) \equiv \phi + (1-\phi)f(r), \tag{6}$$

so that $f(0) = 1$, and $f(\infty) = 0$.

Debye et al. [11] showed that, by scattering of X-ray, the structure factor of many porous media could be described by a single correlation length λ

$$f(r) \approx e^{-(r/\lambda)}, \quad \text{where } \frac{1}{\lambda} = -\frac{S_2'(0)}{1-\phi} = \frac{S}{4V_p(1-\phi)}. \tag{7}$$

In a well sorted, such as a pack of mono-sized beads, one finds other features, such as oscillations in the structure factor. A nice figure which relates various features of $S_2(r)$ to geometrical features, e.g., grain size is given in [10,12].

In the same spirit, we introduce the pair-correlation function $K_2(\mathbf{r})$ for the internal field, B_z. The details of B_z will be discussed in later sections. The correlation functions for other components can be derived using the same technique.

$K_2(\mathbf{r})$ is defined similarly as S_2:

$$K_2(\mathbf{r}) \equiv \frac{\int d\mathbf{r}_1 B_z(\mathbf{r}_1+\mathbf{r})X(\mathbf{r}_1+\mathbf{r})B_z(\mathbf{r}_1)X(\mathbf{r}_1)}{\int d\mathbf{r}_1 X(\mathbf{r}_1+\mathbf{r})X(\mathbf{r}_1)} \tag{8}$$

$$\equiv \frac{C_2(\mathbf{r})}{S_2(\mathbf{r})}. \tag{9}$$

The X factors ensure that only contributions from the pore space is included. This definition is most relevant to NMR experiments that use spins to detect magnetic field changes. The function K_2 is specific to the magnetic field. For example, in a constant field, $K_2 = 1$, independent of distance and $C_2(r) = S_2(r)$.

Again, the material is assumed to be isotropic homogeneous, so that K_2 only depends on the distance r. The factors $X(\mathbf{r}_1+\mathbf{r})X(\mathbf{r}_1)$ are made explicit to show that as $r \to \infty$,

$$C_2(r\to\infty) \to \left(\frac{1}{V_p}\int_{V_p} d\mathbf{r}_1 B_z(\mathbf{r}_1)\right)^2 = \phi\langle B_z\rangle_{V_p}^2. \tag{10}$$

Since the average field is zero, $K_2(r\to\infty) \approx 0$. Similarly,

$$C_2(r\equiv 0) = \frac{1}{V_p}\int_{V_p} d\mathbf{r}_1 B_z(\mathbf{r}_1)^2 = \langle B_z^2\rangle_{V_p}. \tag{11}$$

3. Magnetic length scale

Next consider the characteristic length associated with the magnetic field that corresponds to λ, that of the structure factor, above. To obtain the initial slope we consider a Taylor expansion of C_2 in terms of r:

$$\begin{aligned} C_2(\mathbf{r}\to 0) &= \frac{1}{V_p}\int_{V_p} d\mathbf{r}_1 B_z^2(\mathbf{r}_1) \\ &\quad + \frac{r}{V_p}\hat{\mathbf{r}}\cdot\int_{V_p} d\mathbf{r}_1(\nabla_1 B_z(\mathbf{r}_1))B_z(\mathbf{r}_1) + \mathcal{O}(r^2) \\ &= \langle B_z^2\rangle_{V_p} + \frac{r}{2V_p}\oint_{S_p} dS_p \hat{\mathbf{r}}\cdot\hat{\mathbf{n}}B_z(\mathbf{r}_1)^2 + \mathcal{O}(r^2) \\ &= \langle B_z^2\rangle_{V_p} - \frac{rS}{4V_p}\langle B_z^2\rangle_{S_p} + \mathcal{O}(r^2). \end{aligned} \tag{12}$$

The last step comes from integrating over the pore-side of the interface (a half-space) and noting the directions of the two unit vectors. The above equation can be re-written, in the spirit of Debye [11], as

$$K_2(\mathbf{r}) \approx \langle B_z^2\rangle_{V_p} e^{-(r/\Lambda_M)}, \tag{13}$$

and the magnetic length scale Λ_M is defined as

$$\frac{1}{\Lambda_M} = \frac{S}{4V_p}\left(\frac{\langle B_z^2\rangle_{S_p}}{\langle B_z^2\rangle_{V_p}} - 1\right). \tag{14}$$

The geometrical and structural information, such as the magnetic length scale Λ_M captured by K_2 is likely to be relevant to the fluid transport properties in the materials. In fact, a similar parameter, Λ, has been investigated extensively [13–15] in an effort to provide a direct characterization of the fluid transport from electric measurement. The Λ parameter is defined for for electrical conduction in insulating porous media with conducting fluids in the interstices:

$$\frac{2}{\Lambda} = \frac{\int|\nabla\psi(\mathbf{r})|^2 dS_p}{\int|\nabla\psi(\mathbf{r})|^2 dV_p}, \tag{15}$$

where ψ is the microscopic electrical potential and $\nabla\psi$ is the electric field. These authors have shown that this Λ parameter or length scale plays an essential role in determining the overall conductivity of porous media when there is an additional non-zero interfacial

conductivity and it is related to the permeability for fluid-flow. The equivalence of magnetostatics and electrostatics implies that Λ_M must be similar to Λ (note the factor of two difference in the definitions). This comparison is rigorous in the limiting case when the spheres are perfectly diamagnetic (such as superconductors), the magnetic field lines are confined in the pore-space, and the normal component of $\mathbf{B}$ is zero. In most cases of interest in NMR, the susceptibility contrast between the phases is a small perturbation and field lines penetrate both the phases. Nevertheless, the correlation function with both ends of the measuring ruler inside the pore carries the relevant information of the pore-space geometry.

In the remainder of the paper, we will consider these ideas for a specific, prototypical porous medium, the Finney pack [16]: a dense random packing of non-penetrating spheres. The pack was made experimentally by filling a container with about 8000 ball bearings of the same size and then squeezing and shaking to reach maximum density. This and similar packs were reviewed by Cargill [17].

4. The Finney pack and magnetism

A dense random packing of non-penetrating spheres, shown in Fig. 1, is used here as a prototypical porous medium. It provides a useful model to understand various transport properties.

First, consider a single sphere of permeability μ_{int} of radius R_0 embedded in a medium of permeability μ_{ext} and subjected to an external uniform field $\mathbf{B}_0$ at infinity. The magnetic dipole moment $\mathbf{m}$ of the sphere is:

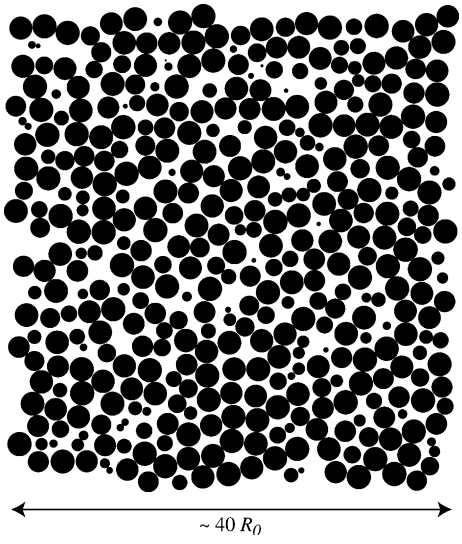

Fig. 1. A typical slice in the Finney pack used for the numerical calculations. The size of the circles depends only on the position of the spheres with respect to the slicing plane.

$$\mathbf{m} = \frac{\mu_{\text{ext}} - \mu_{\text{int}}}{\mu_{\text{ext}} + 2\mu_{\text{int}}} R^3 \mathbf{B}_0. \tag{16}$$

We only consider here a small and isotropic susceptibility for both the spheres and the medium, such that $\mathbf{m}$ is along the direction of $\mathbf{B}_0$, and $\mathbf{m} \approx 4\pi\Delta\chi \mathbf{R}_0^3 B_0/3$, in three dimensions, and $4\pi\Delta\chi = \mu_{\text{ext}} - \mu_{\text{int}}$.

The magnetic field at a point $\mathbf{R}$ due to the magnetic dipole $\mathbf{m}$ located at the origin in three dimensions is (see, for example, Eq. 5.58 in [18]):

$$\mathbf{B}^{\text{int}}(\mathbf{R}) = \frac{3(\mathbf{m}\cdot\mathbf{R})\mathbf{R} - \mathbf{R}^2\mathbf{m}}{|\mathbf{R}|^5}. \tag{17}$$

The total local field is the sum of B_0 and B^{int}. In this article, we shall be only concerned with the internal field, B^{int}.

If we take $\mathbf{B}_0$ along $\hat{z}$, $B_z^{\text{int}} \propto [3\cos^2(\theta) - 1]/|\mathbf{R}|^3$, has positive values at the poles, $\theta = 0, \pi$ and negative at the equators $\theta = \pi/2$. For an isolated dipole, the regions of the strong field are at the north and the south poles. It can be seen that the field gradients are strongly localized near the north and south poles as well as near the rest of the surface. We will see below that some of these features persist while new features emerge in dense packs where the total field is a superposition of the fields from individual spheres.

The internal field at coordinate $\mathbf{R}$ is given by a superposition of fields from all spheres:

$$\mathbf{B}^{\text{int}}(\mathbf{R}) = \sum_i \frac{3\mathbf{m}\cdot(\mathbf{R}-\mathbf{R}_i)(\mathbf{R}-\mathbf{R}_i) - (\mathbf{R}-\mathbf{R}_i)^2\mathbf{m}}{|\mathbf{R}-\mathbf{R}_i|^5} \tag{18}$$

and $\mathbf{R}_i$ are the centers of the spheres.

One can show that some of the properties of the internal field are independent of the sphere size. Let us use a scaled variable, $\mathbf{r}$, so that $\mathbf{R} \equiv \mathbf{r}R_0$. Eq. (18) can be rewritten in term of the scaled variable,

$$\begin{aligned}\mathbf{B}^{\text{int}}(\mathbf{r}) &= \frac{m}{R_0^3}\sum_i \frac{3\hat{z}\cdot(\mathbf{r}-\mathbf{r}_i)(\mathbf{r}-\mathbf{r}_i) - (\mathbf{r}-\mathbf{r}_i)^2}{|\mathbf{r}-\mathbf{r}_i|^5} \\ &= \frac{4\pi\Delta\chi B_0}{3}\sum_i \frac{3\hat{z}\cdot(\mathbf{r}-\mathbf{r}_i)(\mathbf{r}-\mathbf{r}_i) - (\mathbf{r}-\mathbf{r}_i)^2}{|\mathbf{r}-\mathbf{r}_i|^5}.\end{aligned} \tag{19}$$

The last line is obtained using Eq. (16). This explicitly shows that if the sample size and geometry are scaled by a constant factor, the magnetic fields at the corresponding positions would remain the same, for instance, the magnetic field distribution would be the same. Of course, the length scale would be scaled by the same factor. As a result, the magnetic field gradient would be reduced by the same factor. In fact, this property is not limited to spherical grains and is generally true for arbitrary shape. This is a consequence of the equations of magnetostatics, for example, see Chapter 5 of [18].

For the rest of the paper, we shall refer to the internal field in the scaled, unitless form, $\mathbf{B} = \mathbf{B}^{\text{int}}/(4\pi\Delta\chi B_0/3)$ and further focus on the z-component, B_z, since it is more relevant to NMR.

To speed up the calculations, we only retained, in the sum in Eq. (19), the dipoles that are close to the point of observation. The contributions from dipoles further than a cut-off distance $d_{\text{cut-off}}$ were discarded. This amounts to assuming a very large spherical Lorentz cavity for the distribution of point-dipoles and a very large spherical sample [4]. We found that the calculated value of the field become practically insensitive to $d_{\text{cut-off}}$ when $d_{\text{cut-off}}$ was greater than $7R_0$. Therefore, we set $d_{\text{cut-off}} = 7R_0$ in all the following numerical simulations. To avoid edge effects, the pore points within a distance $d_{\text{cut-off}}$ from the boundary of the packing were never scanned. In this way, the spatial distribution of the dipoles contributing in the above sum is always that of a spherical bulk sample. This technique also avoids the demagnetization effect due to finite sample with non-spherical shape.

5. Internal field in the Finney pack

5.1. Distribution and spatial characteristics

In Fig. 2 we show the internal field and the gradient along the YZ plane in the center of the pack. In Fig. 2a where B_z is shown, one can clearly observe the variation of B_z within individual pores and that the overall field change occurs over the length scale of the pore size. For example, there is no rapid oscillation of the field within one pore. In addition, the hot spots continue to be present near the north and the south-poles of many grains. Fig. 2b shows that the magnitude of the gradient $|\nabla B_z|$ is stronger near the poles.

Figs. 2c and d show the distributions of B_z and the magnitude of the gradient $|\nabla B_z|$. The shape of the field

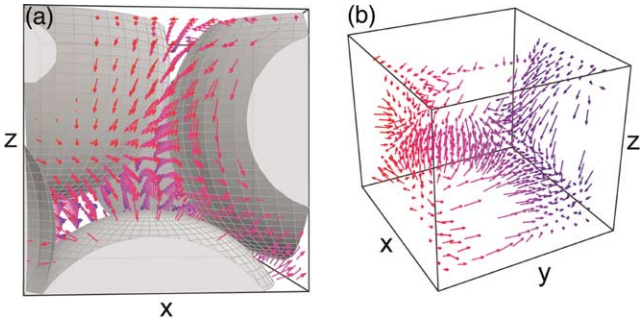

Fig. 3. The internal field **B** vector is shown as arrows in a pore at the middle of the Finney pack. The surfaces of the nearby spheres are shown in (a) to give a sense of the pore space and absent in (b) for a better visualization of the back of the pore. One finds that the flux lines near the spheres are similar to those of the isolated spheres while the flux lines in the middle region of the pore display a complex behavior.

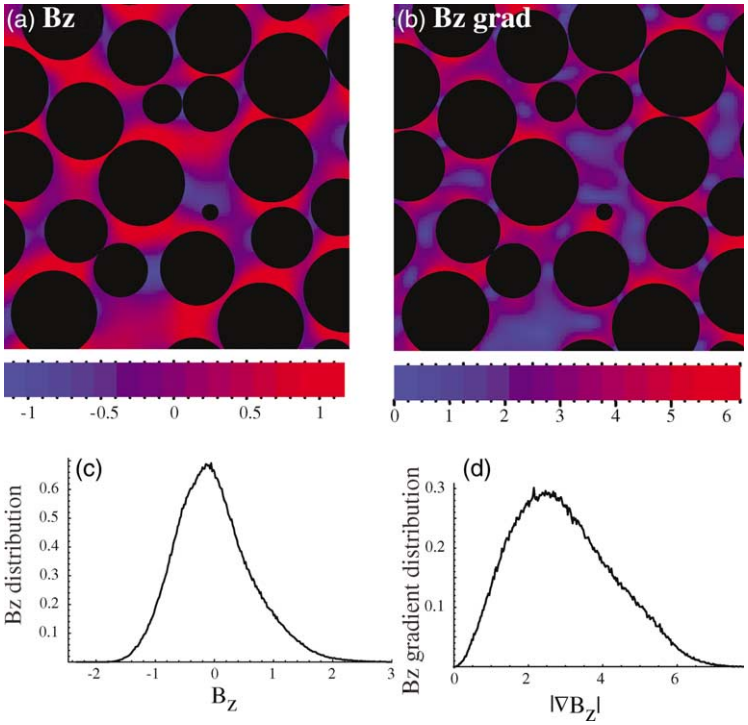

Fig. 2. (a) Internal field (z-component) and (b) the magnitude of its gradient $|\nabla B_z|$ in the Finney pack of spheres, shown along a plane (YZ) in the middle of the pack. The circular black objects are the sections of the spheres and their sizes are dependent on the position of the sectioning plane to the individual spheres. The internal field is shown as the color scale from minimum to maximum values. The external field is applied vertically. (c) Distributions of B_z and (d) the magnitude of the field gradient, $|\nabla B_z|$, of the Finney pack.

distribution is approximately symmetrical, which is very different from that of a single isolated dipole sphere [2]. This is clearly due to the superposition of the field from many spheres. The average field is zero, a reflection of the isotropy of the arrangement of the spheres. It is also very different from that of the 2D cylinder pack [4] where a singularity is present at the zero field. Such singularity also appears in regularly packed spheres in three dimension [19] due to the particular symmetry of the structures. In the randomly packed samples, no long range packing orders exist, as a result, the field distribution appears smooth without sharp features.

Using the original dipole formula for the internal field, Eq. (19), we have calculated the second moment of the field (B_z) distribution

$$\sqrt{\langle B_z^2 \rangle} = 0.642. \tag{20}$$

Note that B_z is a normalized variable and unitless. The second moment is often a good measure of the the range of B_z. It is important to note that the internal field is bound by a maximum and the minimum, which are found numerically to be 3.5 and −1.9. The maximum field is likely to be in the locations where two spheres are close and aligned along the direction of $\mathbf{B}_0$, thus the contributions from the two spheres are added with the maximum of 4 corresponding to two touching spheres. The minimum field corresponds to two spheres nearby and aligned perpendicular to $\mathbf{B}_0$ so that the minimum is −2. Certainly, the range of B_z^{int} as measured in the experiments, and its minimum and maximum fields are proportional to the applied field B_0.

The field gradient also shows a broad distribution, Fig. 2d. Since B_z and its slope are continuously varying in space, such a broad gradient distribution should not be viewed simply as a summation of constant gradients. Instead, it should be considered as a reflection of the complex spatial characteristics of B_z and the full spatial dependence can be very important in many experimental conditions. For example, the gradient is often measured by spin-echo decay or CPMG sequence where the spins are allowed to diffuse certain distance. The measured gradient is in fact averaged over this distance. Thus, when the diffusion distance is changed, the obtained gradient distribution may change.

Fig. 3 shows a three-dimensional view of the internal field vector **B** within one pore in the middle of the Finney pack. The length of the arrows is proportional to the magnitude of $|\mathbf{B}|$ and the direction of the arrow indicates the orientation of the **B** vector. Also, the color of the arrows from red to blue is proportional to the y-coordinate, providing a sense of perspective. Near the spheres, one may find that the flux line of **B** (by connecting the arrows) are similar to those for a single sphere, due to the dominating contribution from the nearest sphere. However, in the rest parts of the pore, contributions from all nearby spheres are important. In the middle region of the pore, the angular dependence of the dipole formula determines that the field, in particular, B_z, will be close to zero due to the near symmetrical contribution from all angles.

5.2. Correlation functions

In Fig. 4, we show correlation functions obtained for the Finney pack. The numerical calculations were performed by the following method. First, pick a point i in the pore space, then select N points randomly and uniformly in the full space (grains and pores). Determine that only N' points (a subset of N) are in the pore space. Thus, $N'/N \to \phi$ when $N \to \infty$. Find the number of points that are at a distance r to the point i from the full space, n, and from the pore space, n'. Then, $S_2(r)$ is given by the assemble average of n'/n when $N \to \infty$ and averaged over i. For K_2, we further calculated the internal magnetic field B_z at all points, and evaluate

$$K_2(r) = \frac{\sum_{ij} B_z(\mathbf{r}_i) B_z(\mathbf{r}_j)}{n'}, \quad j \in n', \text{ and } N \to \infty. \tag{21}$$

For all pairs, $|\mathbf{r}_i - \mathbf{r}_j| = r$. An averaging over i is made.

Despite the broad argument that B_z should reflect the pore geometry in some ways, the similarity of the two functions is striking. Both of them exhibit very similar initial decay at short distance, and several periods of oscillations with a period slightly larger than the diameter

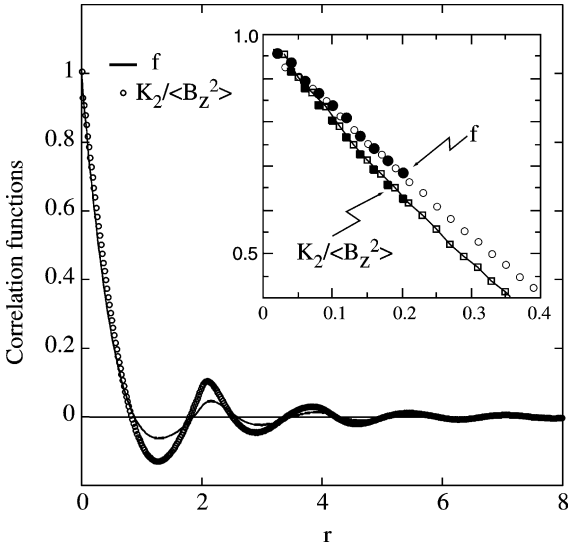

Fig. 4. Plots of the pair-correlation functions of the pore space f (line) and the internal magnetic field, $K_2/\langle B_z^2 \rangle$ (open circles) calculated for the Finney pack. The similarity between the two functions are remarkable. The inset shows the correlation functions for small r and the filled symbols (circles for f and squares for K_2) were data obtained using a specific algorithm to enhance the accuracy at small r. The porosity of Finney pack is found to be 0.361.

of the spheres. The only difference is the amplitude of the oscillation is somewhat larger for K_2 at r around 1–2.

The appearance of the smooth initial decay of K_2 with a slope that is similar to the surface-to-volume ratio is another demonstration of our earlier conclusion from the visualization of B_z that the internal field inhomogeneity occurs over the length scale of the pore size and there is no rapid oscillation of B_z within one pore. This conclusion from K_2 is much stronger because it is based on the statistics of many pores, compared to that from Figs. 2 and 3 which include only a few pores and a limited perspective.

The other important aspect of the similarity between f and K_2 is that the magnetic field correlation function can be experimentally measured by NMR techniques, thus providing a novel method for the determination of the pore structure.

Numerical evaluation for the Finney pack yields $\langle B_z^2\rangle_{S_p} = 0.941$ and $\langle B_z^2\rangle_{V_p} = 0.412$. Using the porosity $\phi = .361$, one obtains $S/V_p = 5.26/R$. The initial slope of f is then $2.07/R_0$, and $1/\Lambda_M = 1.67/R_0$. This value is consistent with a direct evaluation of the slope of $K_2(\mathbf{r})$ in Fig. 4.

6. Conclusion

In this paper, the internal magnetic field induced by the susceptibility contrast are examined with details. We show that a striking similarity between the magnetic field correlation function K_2 to the structure factor of the porous media. As a result, it is likely that K_2 may provide a new possibility using NMR to characterize internal structure of complex media instead of using the conventional scattering technique such as X-ray and neutron.

We would like to summarize the properties of the internal field:

1. B_z^i profile and its distribution is independent of the grain size. When the grain size is scaled up by a factor k while maintaining the overall geometry, the B_z^i profile will remain the same with the distance scaled by the same factor.
2. B_z^i is bounded by a maximum and a minimum.
3. The spatial correlation of B_z^i decays over the length scale of the pore size.
4. B_z^i profile in different pores are similar statistically.
5. The internal field correlation function is intimately related to the structure factor of the medium.
6. The initial decay of the field correlation function characterizes a magnetic length scale Λ_M which is likely to be an important parameter for fluid transport in the medium.

Acknowledgments

We would like to thank Drs. David L. Johnson and Martin D. Hürlimann for insightful discussions.

References

[1] Y.-Q. Song, S. Ryu, P.N. Sen, Determining multiple length scales in rocks, Nature (London) 406 (2000) 178.
[2] R.J.S. Brown, Distribution of fields from randomly placed dipoles: free-precession signal decay as a result of magnetic grains, Phys. Rev. 121 (1961) 1379.
[3] L.E. Drain, The broadening of magnetic resonance lines due to field inhomogeneity in powdered samples, Phys. Soc. Proc. 80 (1962) 1380.
[4] P.N. Sen, S. Axelrod, Inhomogeneity in local magnetic field due to susceptibility contrast, J. Appl. Phys. 86 (1999) 4548.
[5] R.J.S. Brown, P. Fantazzini, Conditions for initial quasilinear $1/T_2$ versus τ for Carr–Purcell–Meiboom–Gill NMR with diffusion and susceptibility differences in porous media and tissues, Phys. Rev. B 47 (1993) 14823.
[6] R.M. Weisskoff, C.S. Zuo, J.L. Boxerman, B.R. Rosen, Microscopic susceptibility variation and transverse relaxation: theory and experiment, Magn. Reson. Med. 31 (1994) 601.
[7] G.C. Borgia, R.J.S. Brown, P. Fantazzini, Scaling of spin-echo amplitudes with frequency, diffusion coefficient, pore size, and susceptibility difference for the NMR of fluids in porous media and biological tissues, Phys. Rev. E 51 (1995) 2104.
[8] M.D. Hürlimann, Effective gradients in porous media due to susceptibility differences, J. Magn. Reson. 131 (1998) 232.
[9] I. Ornstein, F. Zernike, Proc. Acad. Sci. (Amsterdam) 17 (1914) 793.
[10] J.G. Berryman, S.C. Blair, Use of digital image analysis to estimate fluid permeability of porous materials: application of two-point correlation functions, J. Appl. Phys. 60 (1986) 1930.
[11] P. Debye, H.R. Anderson, H. Brumberger, Scattering by an inhomogenous solid. II. The correlation function and its application, J. Appl. Phys. 28 (1957) 679.
[12] P.N. Sen, M.D. Hürlimann, Analysis of nuclear magnetic resonance spin echoes using simple structure factors, J. Chem. Phsys. 101 (1994) 5423.
[13] D.L. Johnson, J. Koplik, L.M. Schwartz, New pore-size parameter characterizing transport in porous media, Phys. Rev. Lett. 57 (1986) 2564.
[14] J.R. Banavar, D.L. Johnson, Characteristic pore sizes and transport in porous media, Phys. Rev. B 35 (1987) 7283.
[15] N. Martys, E.J. Garboczi, Length scales relating the fluid permeability and electrical conductivity in random two-dimensional model porous media, Phys. Rev. B 46 (1992) 6080.
[16] J.L. Finney, Random packing and the structure of the liquid state, Ph.D. thesis, University of London, 1964.
[17] G.S. Cargill, Radial distribution functions and microgeometry of dense random packings of hard spheres, in: D.L. Johnson, P.N. Sen (Eds.), Physics and Chemistry of Porous Media, American Institute of Physics, New York, 1984.
[18] J.D. Jackson, Classical Electrodynamics, second ed., Wiley, New York, 1962.
[19] P.N. Sen, B. Audoly, S. Axelrod, Inhomogeneity in Local Magnetic Field due to Susceptibility Contrast, presented at Experimental NMR Conference, 1999.